Radiation Damage from Neutron Scattering

Sebastian Schunert, Marina Sessim, Daniel Schwen

Fuels Modeling and Simulation Department, Idaho National Laboratory, P.O Box 1625, Idaho Falls, ID 83415

Abstract

Keywords: Radiation damage, Elastic scattering, Inelastic scattering

1. Introduction

The purpose of this report is to derive expressions for the elastic and inelastic neutron recoil cross sections dependent only on quantities that can be obtained easily from fundamental data such as the National Nuclear Data Center [1]. Recoil cross sections are essential to compute isotope, angle and energy dependent recoil rates given detailed neutron distribution in phase space that can be computed by a radiation transport code. In particular, the recoil cross sections are used in the Rattlesnake radiation transport code [2] to compute recoil rate distributions that are passed on to the Magpie glue application for computing primary knock-on atom (PKA) distribution rates in turn used for coupled binary-collision Monte-Carlo/FEM calculations. Elastic and inelastic neutron scattering events are important interactions initiating radiation damage cascades especially in structural materials.

2. Scattering Kinematics

Following Fig. 1, we denote the speed of the neutron by v and the speed of the recoil atom as V. The subscript shall denote in which frame of reference the speed is measured, v_l is measured in the laboratory (LAB) frame and v_c is measured in the center of mass (CM) frame. Primed speeds, e.g. v_c', denote states after the collision, while un-primed speeds denote states prior to the

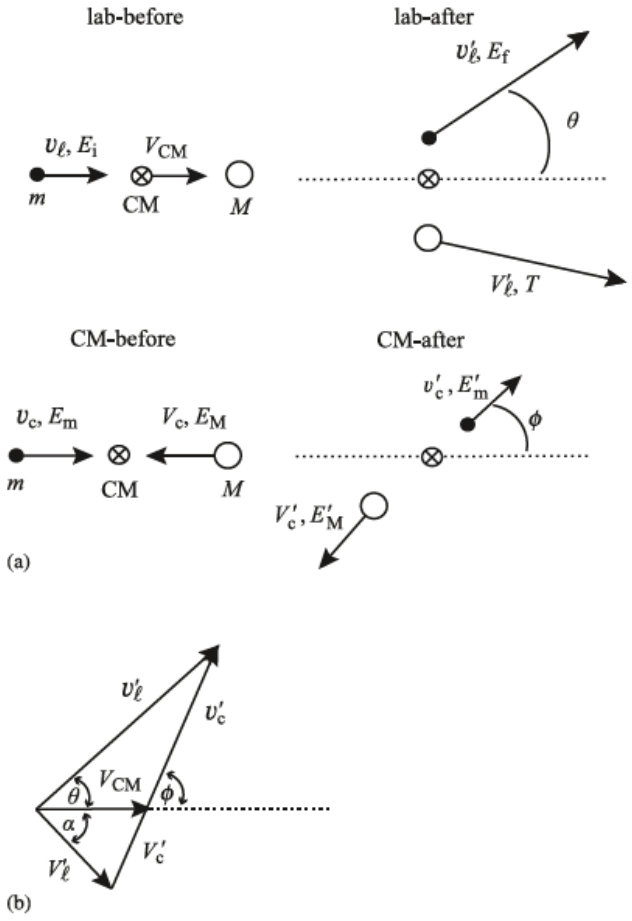

Figure 1: Relationship between angles in CM and laboratory frame [3].

collision. The scattering angle in the CM frame is denoted by ϕ, while the recoil angle in the LAB frame is denoted by α. We denote the cosine of these angles as $\mu_l = \cos\alpha$ and $\mu_c = \cos\phi$. Within the following development, some expressions hold for both elastic and inelastic scattering, while some hold only for one of them. We shall adopt the convention that unless otherwise stated, expressions hold for both elastic and inelastic scattering.

2.1. Relationship between Recoil Angles in CM and LAB frames

First, we point out that the mass of the of the neutron is set to unity $m = 1$, while the mass of the recoil atom is its mass number $M = A$. The speed of the center of mass v_{CM} is given by [4]:

The velocity of the center of mass v_{CM} is given by [4]:

$$v_{CM} = \frac{1}{m+M}(mv_l + MV_l) = \left(\frac{1}{1+A}\right) v_l \tag{1}$$

The relationship between the velocities on the LAB and CM frame is given by:

$$v_c = v_l - v_{CM} = \frac{A}{A+1} v_l \tag{2}$$

and

$$V_c = -v_{CM} = \frac{1}{A+1} v_l \tag{3}$$

where we have assumed that the target nucleus is at rest before the collision.

2.1.1. Elastic Scattering

Following [3] we can formulate energy and momentum conservation in the CM frame:

$$\begin{aligned} v_c - V_c A &= 0 \\ v'_c - V'_c A &= 0 \\ \frac{1}{2}v_c^2 + \frac{1}{2}AV_c^2 &= \frac{1}{2}v_c'^2 + \frac{1}{2}AV_c'^2. \end{aligned} \tag{4}$$

From Eq. 4 we can conclude:

$$\begin{aligned} V_c &= V'_c \\ v_c &= v'_c, \end{aligned} \tag{5}$$

which is a well known result stated by [4] as (paraphrasing): the magnitude of the CM velocities of the projectile and target are not changed but only rotated. From Eq. 5 and Eq. 3 it follows that $|V'_c| = |v_{CM}|$.

Focusing on the triangle spanned by v_{CM}, V_l', and V_c' in Fig. 1 (b), we realize that the triangle is isosceles because $|V_c'| = |v_{CM}|$. Hence, we have:

$$\phi + 2\alpha = \pi \rightarrow \alpha = \frac{1}{2}(\pi - \phi). \tag{6}$$

Taking the cosine on both sides leads to:

$$\mu_l = \cos\left(\frac{\pi}{2} - \frac{\phi}{2}\right) = \sin\frac{\phi}{2} = \pm\sqrt{\frac{1-\cos\phi}{2}} = \pm\sqrt{\frac{1-\mu_c}{2}}. \tag{7}$$

Finally, we need to specify which sign in Eq. 7 is correct. The recoil angle in the LAB frame α must be between 0 and $\phi/2$, i.e. the recoil atom cannot be backscattered. Hence, $\mu_l > 0$ and we find that:

$$\mu_l = \sqrt{\frac{1-\mu_c}{2}}. \tag{8}$$

2.2. Inelastic Scattering

The relationship between CM and LAB angles is more complicated for inelastic scattering because the triangle spanned by v_{CM}, V_l', and V_c' in Fig. 1 (b) is *not* isosceles. From the same triangle, we infer by simple geometric considerations along the x and y directions:

$$\begin{aligned} \sin\alpha\ V_l' &= \sin\phi\ V_c' \\ \cos\alpha\ V_l' &= v_{CM} - \cos\phi\ V_c'. \end{aligned} \tag{9}$$

Taking the ratio of the first and second Eq. 9 gives:

$$\tan\alpha = \frac{\sin\phi}{\frac{V_c}{V_c'} - \cos\phi}. \tag{10}$$

It now remains to determine the ratio V_c/V_c'. To this end, the energy and momentum balance Eq. 4 is extended to inelastic scattering by introducing the Q-value of the reaction Q_j, where j indicates the excitation level a particular inelastic scattering event triggers:

$$\begin{aligned} v_c - V_c A &= 0 \\ v_c' - V_c' A &= 0 \\ Q_j + \frac{1}{2}v_c^2 + \frac{1}{2}AV_c^2 &= \frac{1}{2}v_c'^2 + \frac{1}{2}AV_c'^2, \end{aligned} \tag{11}$$

where $Q_j < 0$. From 11 we derive the following relationship between V_c and V_c':

$$V_c'^2 = V_c^2 + \frac{2Q_j}{A(A+1)} \rightarrow \left(\frac{V_c'}{V_c}\right)^2 = 1 + \frac{2Q_j}{A(A+1)V_c^2}. \tag{12}$$

The square oif the initial velocity V_c^2 can can be replaced by the v_l using Eq. 3:

$$V_c^2 = \frac{2}{(A+1)^2}\frac{1}{2}v_l^2 = \frac{2E}{(A+1)^2}, \tag{13}$$

where E is the initial energy of the neutron in the LAB frame. Finally we obtain:

$$\left(\frac{V_c}{V_c'}\right) = \left(1 + \frac{Q_j}{E}\frac{A+1}{A}\right)^{-1/2}. \tag{14}$$

Introducing the threshold energy E_t and the dimensionless neutron energy Δ by:

$$\begin{aligned} E_t &= \frac{(A+1)}{A}\left|Q_j\right| \\ \Delta &= \frac{E_t}{E}, \end{aligned} \tag{15}$$

we can simplify Eq. 14 to:

$$\left(\frac{V_c}{V_c'}\right) = (1-\Delta)^{-1/2}. \tag{16}$$

Using Eq. 16 in Eq. 10 gives:

$$\tan\alpha = \frac{\sin\phi}{(1-\Delta)^{-1/2} - \cos\phi}. \tag{17}$$

We now want to write the right hand side of Eq 17 in terms of μ_c. First, we note that $\sin\phi \geq 0$ because $0 \leq \phi \leq \pi$. Hence, we can replace $\sin\phi$ with $\sqrt{1-\mu_c^2}$ as opposed to using the opposite sign. For convenience we denote the right hand side of Eq 17 as $f(\mu_c)$:

$$f(\mu_c) = \frac{\sqrt{1-\mu_c^2}}{(1-\Delta)^{-1/2} - \mu_c}, \tag{18}$$

Note that since $0 < \Delta \leq 0$, $(1-\Delta)^{-1/2} \geq 1$ and consequently $f(\mu_c) > 0$. Writing Eq. 17 in terms of μ_l gives:

$$\mu_l = \sqrt{\frac{1}{1+f^2(\mu_c)}}, \tag{19}$$

where we immediately asserted $\mu_l > 0$ when taking the square root.

3. Energy Transfer to the Recoil Nucleus - Elastic Scattering

In this section, we derive the relationship between the energy of the neutron prior to the collision E, the energy of the recoil nucleus after the collision T, and the scattering cosine in the CM frame μ_c. If two of the three quantities are given, the third is determined and can no longer be chosen at will. It is convenient to define the mass fraction γ [3]:

$$\gamma = \frac{4A}{(A+1)^2} \tag{20}$$

[Note this mass fraction is universally applicable to elastic and inelastic scattering even though it is contained in the elastic scattering energ transfer section.] For elastic scattering, the relationship between E, T and μ_c is given by [3]:

$$T = \frac{\gamma}{2}E(1-\mu_c). \tag{21}$$

Solving for μ_c gives:

$$\mu_c = 1 - \frac{2T}{\gamma E} \tag{22}$$

4. Energy Transfer to the Recoil Nucleus - Inelastic Scattering

The following expression is adopted from [3]:

$$T = \frac{\gamma}{2}E - \frac{\gamma}{2}\left[E\left(E + Q_j\frac{A+1}{A}\right)\right]^{1/2}\mu_c + \frac{Q_j}{A+1}, \tag{23}$$

where it is again stressed that $Q_j < 0$. We can rewrite this equation in a more convenient form by using the dimensionless neutron energy Δ:

$$T = \frac{\gamma}{2}E\left(1 - \mu_c\sqrt{1-\Delta} - \frac{1}{2}\Delta\right). \tag{24}$$

5. Limits on the Scattering Angles and Energy Transfer

5.1. Scattering Angle in CM

It is obvious from Fig. 1 (b) that the scattering angle in the CM frame ϕ satisfies:

$$0 \leq \phi \leq \pi. \tag{25}$$

An angle $\phi > \pi$ would simply reflect Fig. 1 (b) about the x-axis. It follows that

$$-1 \leq \mu_c \leq 1. \tag{26}$$

5.2. Recoil Angle in LAB

The recoil angle in the LAB frame must be between 0 and $\pi/2$:

$$0 \leq \alpha \leq \pi/2. \tag{27}$$

This can most easily be seen when considering the triangle V_l', v_{CM}, V_c' in Fig. 1 (b). For both elastic and inelastic scattering we see from Eq. 14 that $V_c' \leq V_c = v_{CM}$. Hence, regardless of the CM scattering angle ϕ with $0 \leq \phi \leq \pi$ the vertex opposite of v_{CM} can never be located to the left of the vertex opposite V_c' proving the limits stated above.

5.3. Recoil Energy for Elastic Scattering

The case $\phi = 0$ ($\mu_c = 1$) corresponds to a grazing collision where the neutron loses no energy and recoil nucleus remains at rest; while $\phi = \pi$ ($\mu_c = -1$) corresponds to a head on collision, where the neutron loses the maximum amount of energy and the recoil receives the maximum amount of energy. Using Eq. 21 with $\mu_c = 1$ and $\mu_c = -1$ gives:

$$0 \leq T \leq \gamma E. \tag{28}$$

5.4. Threshold Neutron Energy, and Recoil Energy for Inelastic Scattering

Neutrons with $\Delta > 1$ cannot cause inelastic scattering reactions. This is consistent with square root terms of the form $\sqrt{1-\Delta}$ which would become imaginary if $\Delta > 1$. However, a more stringent requirement is that the CM scattering cosine is within physical bounds $-1 \leq \mu \leq 1$. For $E \to E_t$ from above, μ_c is strictly monotonically decreasing. Given an arbitrary value of the recoil energy T, $\mu_c = -1$ is usually not assumed for $E = E_t$. The minimum possible neutron energy for a given recoil energy is:

$$E_{min}(T) = \frac{(T(A+1) + |Q_j|)^2}{4AT}. \tag{29}$$

Further analysis shows that E_{min} assumes a minimum at:

$$T = \frac{|Q_j|}{A+1}, \tag{30}$$

where we have

$$E_{min}(\frac{|Q_j|}{A+1}) = E_t. \tag{31}$$

The maximum and minimum energy of the recoil are denoted by $T_{min}(E)$ and $T_{max}(E)$ and they occur for $\mu_c = 1$ and $\mu_c = -1$, respectively. For convenience we define:

$$g(\mu_c, \Delta) = \frac{\gamma}{2} E \left(1 - \mu_c \sqrt{1-\Delta} - \frac{1}{2}\Delta\right). \tag{32}$$

The function $g(\mu_c, \Delta)$ is plotted for $\mu_c = 1$ and $\mu_c = -1$ in Fig. 2. The maximum and minimum recoil energy given a neutron energy are given by:

$$\begin{aligned} T_{min}(E) &= \frac{\gamma}{2} E \left(1 - \sqrt{1-\Delta} - \frac{1}{2}\Delta\right) \\ T_{max}(E) &= \frac{\gamma}{2} E \left(1 + \sqrt{1-\Delta} - \frac{1}{2}\Delta\right). \end{aligned} \tag{33}$$

It should be noted that T_{min} and T_{max} are monotonically decreasing and increasing with neutron energy E, respectively.

5.5. Limits of Inleastic Scattering Energies considering Neutron and Recoil Energy Bins

In this section we consider the case, where neutron and recoil energy limits are desired for a transfer of neutrons with energies $E_l \leq E \leq E_u$ causing recoils with energies $T_l \leq T \leq T_u$. The final energy limits shall be denoted by $E_\downarrow$, $E_\uparrow$, $T_\downarrow$, and $T_\uparrow$ for the lower and upper energy limits of the neutron and recoil, respectively. These limits denote possible scattering interactions consistent with the energy group boundaries. To illustrate the recoil energy limits, we consider Fig. 3. The curves representing $T_{min}(E)$ and $T_{max}(E)$ are depicted in green and blue, respectively. They share a common point at $E = E_t$, $T = \frac{|Q_j|}{A+1}$ with a common vertical tangent $E = E_t$ depicted in red. The energy group boundaries E_l, E_u, T_l and T_u are depicted in orange.

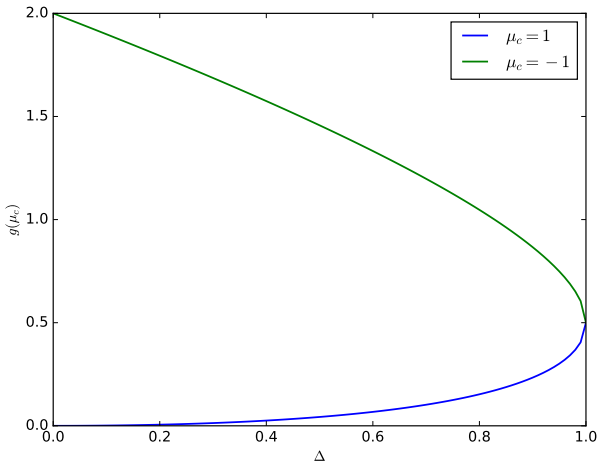

Figure 2: Function $g(\mu_c, \Delta)$ plotted vs. Δ for $\mu_c = 1$ (minimum recoil) and $\mu_c = -1$ (maximum recoil).

The limits on the neutron energy are:

$$E_\downarrow = \begin{cases} E_l, & E_l > E_t \\ E_t, & E_l \leq E_t \end{cases}$$
$$E_\uparrow = \begin{cases} E_u, & E_l > E_t \\ \text{neutrons cannot scatter}, & E_u \leq E_t \end{cases} . \tag{34}$$

In Fig. 3 $E_t < E_l < E_u$ and hence $E_\downarrow = E_l$ and $E_\uparrow = E_u$. The range of possible recoil energies is given by the overlap of two areas: first, the range $[T_l, T_u]$ and second the physically possible minimum and maximum recoil energies $[T_{min}, T_{max}]$. The upper limit is given by:

$$T_\uparrow = \min\left(T_{max}(E_\uparrow), T_u\right). \tag{35}$$

Note that the largest value of T_{max} is assumed for the largest E. The lower limit is given by:

$$T_\downarrow = \max\left(T_{min}(E_\uparrow), T_l\right). \tag{36}$$

Again it should be noted that the minimum of T_{min} is assumed for the largest neutron energy. In Fig. 3 the region of permissible scattering is marked by

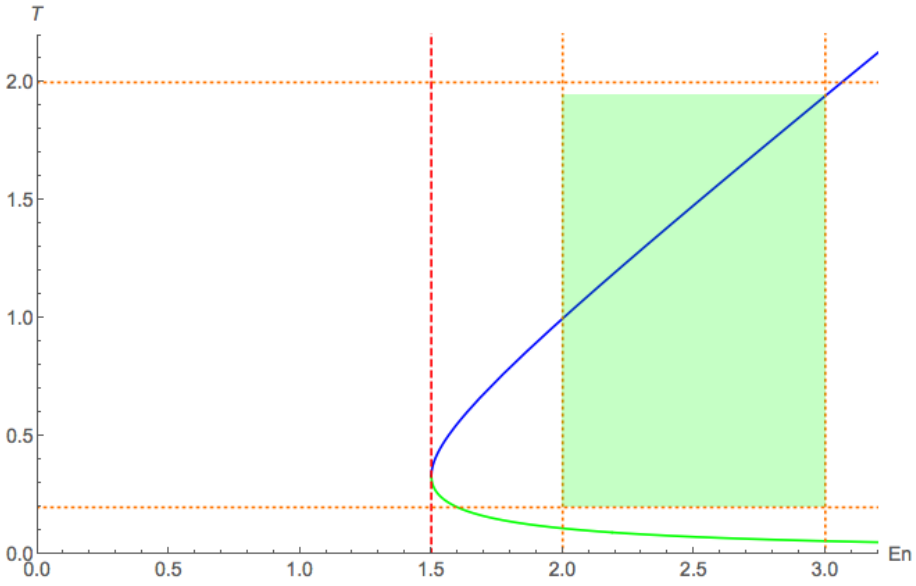

Figure 3: Diagram in E-T space to illustrate limits on recoil energy.

the green box. It should be noted that the fraction of the scattering processes located in the green box but above the blue T_{max} line are impossible which must be taken into consideration when a particular $E \to T$ set is considered. Finally, the scattering process is impossible if:

$$\begin{aligned} E_u &< E_t \\ \text{or } T_\uparrow &< T_l \\ \text{or } T_\downarrow &> T_u. \end{aligned} \tag{37}$$

5.6. Limits of the Scattering Cosine in the LAB Frame

In case of elastic scattering, μ_l is strictly monotonically decreasing with μ_c and μ_c is strictly monotonically decreasing with the ratio T/E. Hence, the limits of μ_l are given by the smallest and largest ratios $T_\downarrow/E_\uparrow$ and $T_\downarrow/E_\uparrow$, respectively:

$$\begin{aligned} \mu_{l,min} &= \mu_{l,min}(E_\uparrow, T_\downarrow) \\ \mu_{l,max} &= \mu_{l,min}(E_\downarrow, T_\uparrow). \end{aligned} \tag{38}$$

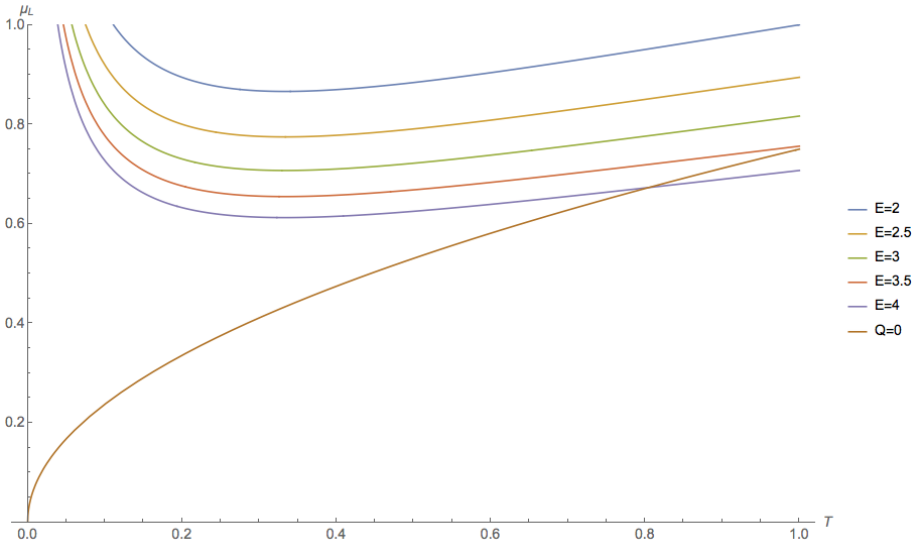

Figure 4: Scattering cosine in the LAB frame μ_l plotted versus recoil energy T for various neutron energies E and $Q = 1$, $A = 2$. For comparison, the case $Q = 0$ is plotted as well.

In the case of inelastic scattering, μ_l can exhibit local minima with respect to T as depicted in Fig. 4. The minimum of the curves in Fig. 4 is assumed at $T = \frac{|Q_j|}{A+1}$ and the minimum recoil cosine in the LAB frame is given by $\sqrt{\Delta}$.

We now describe how to determine $\mu_{l,\downarrow}$ and $\mu_{l,\uparrow}$ if the neutron and recoil energies are limited by $E_\downarrow$, $E_\uparrow$, $T_\downarrow$, and $T_\uparrow$. It is useful to note that in Fig. 4 curves with larger E are located below curves with smaller E. Hence, in order to obtain $\mu_{l,\uparrow}$, we use $E = E_\downarrow$. The value at which the $\mu_{l,\uparrow}$ is assumed is then given by:

$$\mu_{l,\uparrow} = \max\left(\mu_l(E_\downarrow, T_\downarrow), \mu_l(E_\downarrow, T_\uparrow)\right). \tag{39}$$

Determining $\mu_{l,\downarrow}$ is slightly more difficult because we need to determine if the minimum is comprised within the range $[T_\downarrow, T_\uparrow]$. If the minimum is not contained, we simply use the value is located closest to the minimum to evaluate

μ_l:

$$\mu_{l,\downarrow} = \begin{cases} \sqrt{\frac{E_t}{E_\uparrow}}, & T_\downarrow \leq \frac{|Q_j|}{A+1} \leq T_\uparrow \\ \mu_l(E_\uparrow, T_\downarrow), & T_\downarrow > \frac{|Q_j|}{A+1} \\ \mu_l(E_\uparrow, T_\uparrow), & T_\uparrow < \frac{|Q_j|}{A+1} \end{cases} . \tag{40}$$

6. Role of De-excitation Gamma Rays

The de-excitation gamma ray is released by the nucleus after the inelastic scattering event concludes. The process of inelastic scattering, considered from before the interaction to after the gamma is released, is a three-body problem. However, as the gamma ray is released after the neutron capture, compound nucleus formation, and neutron release it can be broken up into two two-body problems. The kinematics of the first two-body problem are discussed above, while the second two-body problem is discussed in this section. The central question is whether the momentum of the de-excitation gamma is large compared to the overall momentum in the system.

The absolute value of momentum of the gamma ray is:

$$|p_\gamma| = \frac{|Q_j|}{c}, \tag{41}$$

where c is the speed of light. The momentum of the neutron prior to collision is:

$$|p_n| = \sqrt{2Em_n}, \tag{42}$$

where m_n is the mass of the neutron. Since $E > \frac{|Q_j|(A+1)}{A} > |Q_j|$, we conclude:

$$|p_n| > \sqrt{2|Q_j|m_n}. \tag{43}$$

For the ratio $r = |p_n|/|p_\gamma|$ it follows that:

$$r > c\sqrt{\frac{2m_n}{|Q_j|}}. \tag{44}$$

Substituting $c \approx 3 \times 10^8$ m/s and $m_n \approx 1.7 \times 10^{-27}$ kg and rounding generously we obtain:

$$r \gtrapprox 42,000\sqrt{\frac{1}{|Q_j|(\text{eV})}} \tag{45}$$

Typical values for E_t, $|Q_j|$, and the lower limit of r are compiled in Table 1. It is obvious that even for the highest threshold energies the momentum in the neutron are much larger than the momentum imparted into the de-excitation gamma ray. As a rule of thumb, the Q-value for inelastic scattering reactions is higher for light nuclides. As light nuclides receive high recoils from elastic scattering reactions and at the same time allow only a fraction of the neutrons to interact with them in the inelastic scattering mode, inelastic scattering is relatively unimportant for light nuclei. Conversely, heavy nuclides do not allow energy transfer by elastic scattering, but have low threshold energies making inelastic scattering important. However, for heavy nuclei the momentum of the gamma ray is even smaller than in the case of light nuclei. In conclusion, the momentum of the gamma ray is small for all cases compared with the overall momentum in the system, but it tends to be smallest for cases where inelastic scattering matters most. Hence, for the purpose of simulating inelastic scattering reactions, the secondary de-excitation can be ignored when determining the direction of the recoil nucleus.

Table 1: Threshold energies, Q-values, and neutron to gamma momentum ratios for several nuclides.

Nuclide	E_t (MeV)	$\|Q_j\|$ (MeV)	r_{min}
^{12}C	4.4	4.15	20
^{16}0	6.1	5.74	17.5
^{23}Na	0.45	0.43	64
^{238}U	0.045	0.045	198

7. Recoil Production Rate

The number of recoils of nuclide type n, with recoil energies in dT about T, and directions within $d\hat{\Omega}_T$ about $\hat{\Omega}_T$ is denoted by $R_n(T, \hat{\Omega}_T)$. It can be

computed by:

$$R_n(T, \hat{\Omega}_T) = N_n \int_{4\pi} d\hat{\Omega} \int_0^{\infty} dE \sigma_{r,n}(E \to T, \hat{\Omega} \to \hat{\Omega}_T) \psi(E, \hat{\Omega}), \tag{46}$$

where N_n is the number density of nuclide n, E is the incident neutron energy, T is the energy transferred to the recoil atom, $\hat{\Omega}$ is the incident neutron direction, $\hat{\Omega}_T$ is the scattered neutron direction, ψ is the angular neutron flux, and $\sigma_{r,n}(E \to T, \hat{\Omega} \to \hat{\Omega}_T)$ is the microscopic, double differential recoil cross section for nuclide n. It will be the overarching task of this section to derive a viable expression for $R_n(T, \hat{\Omega}_T)$ in terms of fundamental properties.

In the vast majority of materials, the recoil cross section only depends on the cosine of the angle between incident neutron direction and recoil direction, i.e. $\mu_l = \hat{\Omega} \cdot \hat{\Omega}_T$ [5]. Consequently, we can rewrite the cross section as: $\sigma_{r,n}(E \to T, \mu_l)$.

Consistent with the multigroup formalism for treating energy dependence of neutron populations, the energy range of the recoils are broken up into groups indexed by $j = 1, ..., J$; consistent with treatment of neutrons the energy groups are numbered in order of descending energy, i.e. the highest energy group has index j, while the lowest energy group has index J. The j-th group comprises the energy range $T_{j+1} \leq T < T_j$. Similarly, neutron energy groups are introduced indexed by $g = 1, ..., G$ following the same convention. Integrating Eq. 46 over the energy range of recoil group j leads:

$$R_{n,j}(\hat{\Omega}_T) = N_n \int_{4\pi} d\hat{\Omega} \int_{T_{j+1}}^{T_j} dT \int_0^{\infty} dE \sigma_{r,n}(E \to T, \mu_l) \psi(E, \hat{\Omega}). \tag{47}$$

The integral over all neutron energies is broken up into contributions from each neutron energy group:

$$R_{n,j}(\hat{\Omega}_T) = N_n \sum_{g=1}^{G} \int_{4\pi} d\hat{\Omega} \int_{T_{j+1}}^{T_j} dT \int_{E_{g+1}}^{E_g} dE \sigma_{r,n}(E \to T, \mu_l) \psi(E, \hat{\Omega}). \tag{48}$$

In the neutron multigroup framework, only the group fluxes $\psi_g(\hat{\Omega})$ are available:

$$\psi_g(\hat{\Omega}) = \int_{E_{g+1}}^{E_g} dE\psi(E,\hat{\Omega}). \tag{49}$$

The recoil rate can formally be written in terms of ψ_g:

$$\begin{aligned} R_{n,j}(\hat{\Omega}_T) &= N_n \sum_{g=1}^{G} \int_{4\pi} d\hat{\Omega}\sigma_{r,n}^{g\to j}(\mu_l)\psi_g(\hat{\Omega}) \\ \sigma_{r,n}^{g\to j}(\mu_l) &= \frac{\int_{T_{j+1}}^{T_j} dT \int_{E_{g+1}}^{E_g} dE\sigma_{r,n}(E\to T,\mu_l)\psi(E,\hat{\Omega})}{\psi_g(\hat{\Omega})}. \end{aligned} \tag{50}$$

during the preparation of the cross sections, the spectrum, i.e. $\psi(E,\hat{\Omega})$, is unknown and hence we need to guess a spectrum that we denote by $\xi(E)$. Using the approximated spectrum, we can approximate $\sigma_{r,n}^{g\to j}(\mu_l)$:

$$\begin{aligned} \sigma_{r,n}^{g\to j}(\mu_l) &\approx \frac{1}{\xi_g} \int_{T_{j+1}}^{T_j} dT \int_{E_{g+1}}^{E_g} dE\sigma_{r,n}(E\to T,\mu_l)\xi(E) \\ \xi_g &= \int_{E_{g+1}}^{E_g} dE\xi(E). \end{aligned} \tag{51}$$

It is convenient to represent the dependence of $\sigma_{r,n}^{g\to j}$ on μ_l as a series expansion in Legendre polynomials truncated at a sufficently high order L:

$$\sigma_{r,n}^{g\to j}(\mu_l) = \sum_{k=0}^{L} \frac{(2k+1)}{\Delta\mu_l}\sigma_{r,n,l}^{g\to j}P_k^*(\mu_l)H(\mu_l,\mu_{l,min},\mu_{l,max}), \tag{52}$$

where $\mu_{l,min}$ and $\mu_{l,max}$ are minimum and maximum LAB scattering cosines for energy group combination g to j (note, these are *not* 0 and 1 corresponding to $\alpha = \pi/2$ and $\alpha = 0$ respectively), $\Delta\mu_l = \mu_{l,max} - \mu_{l,min}$, $P_l^*(\mu_l) = P_l\left(2\frac{\mu_l-\mu_{l,min}}{\Delta\mu_l} - 1\right)$ with P_k being standard Legendre polyonomials of order k of which the first few are $1, \mu_l, 1/2(3\mu_l^2-1), ...$, and finally $H(\mu_l,\mu_{l,min},\mu_{l,max})$ is given by:

$$H(\mu_l,\mu_{l,min},\mu_{l,max}) = \begin{cases} 1 & \mu_{l,min} \le \mu_l \le \mu_{l,max}; \\ 0 & \text{else.} \end{cases} \tag{53}$$

The Legendre polynomials satisfy the following orthogonality property:

$$\int_{\mu_{l,min}}^{\mu_{l,max}} d\mu_l P_k^*(\mu_l) P_i^*(\mu_l) = \frac{\Delta\mu_l}{2k+1}\delta_{k,i}, \tag{54}$$

where $\delta_{k,i}$ is the Kronecker delta. For elastic scattering, the minimum and maximum scattering cosines in the LAB frame can be determined from the smallest and largest T/E ratio for pairing g and j as follows:

$$\begin{aligned}\left(\frac{T}{E}\right)_{min} &= \left(\frac{T_{j+1}}{E_g}\right) \rightarrow \mu_{c,max} \rightarrow \mu_{l,min} \\ \left(\frac{T}{E}\right)_{max} &= \left(\frac{T_j}{E_{g+1}}\right) \rightarrow \mu_{c,min} \rightarrow \mu_{l,max},\end{aligned} \tag{55}$$

where Eqs. 22 and 8 are used for elastic scattering and Eqs. 24 and 19 are used for inelastic scattering. For inelastic scattering the equations in section 5.6 are used.

Multiplying Eq. 52 with P_i^* and integrating over μ_l within $\mu_{l,min}$ and $\mu_{l,max}$ gives:

$$\sigma_{r,n,l}^{g\rightarrow j} = \int_{\mu_{l,min}}^{\mu_{l,max}} d\mu_l P_i^*(\mu_l)\sigma_{r,n}^{g\rightarrow j}(\mu_l). \tag{56}$$

Before continuing, the dependence of the recoil cross section on T, E and μ_l is discussed. In section 2.1 we determined a relationship of the scattering cosine in the LAB and CM frame, where for elastic scattering μ_l is a function of μ_c only, while for inelastic scattering μ_l also depends on E. As pointed out previously T, E and μ_c cannot all be chosen independently, rather if two are chosen the third follows. From the last two statements it follows that out of T, E and μ_l only two can be independently chosen. Further, the cross section is usually split into a energy dependent total recoil cross section $\sigma_{r,n}(E)$ and a probability distribution function $\mathcal{P}(E \rightarrow T)$ describing the likelihood of a transfer from neutron energy E to recoil energy T. The double differential scattering crosss section can consequently be written as:

$$\sigma_{r,n}(E \rightarrow T, \mu_l) = \sigma_{r,n}(E)\mathcal{P}(E \rightarrow T)\delta(\mathcal{T}(\mu_l) - T), \tag{57}$$

where δ is the Dirac delta function and $\mathcal{T}(\mu_l)$ is the recoil energy obtained from compositions of Eqs. 22 and 8 and Eqs. 24 and 19 for elastic and inelastic scattering, respectively. Now substituting Eq. 57 into Eq. 51 and this result into Eq. 56 leads to:

$$\sigma_{r,n,l}^{g\to j} = \frac{1}{\xi_g} \int_{T_{j+1}}^{T_j} dT \int_{E_{g+1}}^{E_g} dE \xi(E) \sigma_{r,n}(E) \mathcal{P}(E \to T) \times \int_{\mu_{l,min}}^{\mu_{l,max}} d\mu_l P_i^*(\mu_l) \delta(\mathcal{T}(\mu_l) - T). \tag{58}$$

Defining μ_l^* implicitly by $T = \mathcal{T}(\mu_l^*)$ we obtain by the virtue of the definition of Dirac's delta function:

$$\sigma_{r,n,l}^{g\to j} = \frac{1}{\xi_g} \int_{T_{j+1}}^{T_j} dT \int_{E_{g+1}}^{E_g} dE \xi(E) \sigma_{r,n}(E) \mathcal{P}(E \to T) P_i^*(\mu_l^*). \tag{59}$$

In general, the distribution function $\mathcal{P}(E \to T)$ is not known, but the scattering law $\mathcal{S}(\mu_c)$ is known. These distributions are related by:

$$\mathcal{P}(E \to T) = \mathcal{S}(\mu_c(E,T)) \left| \frac{d\mu_c}{dT} \right|. \tag{60}$$

Hence:

$$\sigma_{r,n,l}^{g\to j} = \frac{1}{\xi_g} \int_{T_{j+1}}^{T_j} dT \int_{E_{g+1}}^{E_g} dE \xi(E) \sigma_{r,n}(E) \mathcal{S}(\mu_c^*) \left| \frac{d\mu_c}{dT} \right| P_i^*(\mu_l^*), \tag{61}$$

where μ_c^* is the CM scattering cosine associated with μ_c^* by Eqs. 8 and 19 for elastic and inelastic scattering, respectively. Finally, we provide expressions for $|d\mu_c/dT|$:

$$\begin{aligned} \text{elastic:} \quad & \left| \frac{d\mu_c}{dT} \right| = \frac{2}{\gamma E} \\ \text{inelastic:} \quad & \left| \frac{d\mu_c}{dT} \right| = \frac{2}{\gamma E \sqrt{1-\Delta}}. \end{aligned} \tag{62}$$

8. Numerical Implementation for Computing Elastic Scattering Cross Sections

The computation of the recoil cross section is implemented in Magpie. The corresponding object takes the following inputs:

- Atomic mass A of the isotope [a.m.u.].
- Neutron energy group boundaries [eV] (array).
- Recoil energy group boundaries [eV] (array).
- Neutron spectrum $\xi(E)$ (Moose function with time t representing energy).
- Neutron elastic cross section data as a funcion of E, $\sigma_{r,n}(E)$ [barn] (Moose function with time t representing energy).
- Scattering law $\mathcal{S}(\mu_c)$ (Moose function with time t representing μ_c).

The object computes the Legendre polynomial coefficients $\sigma_{r,n,l}^{g\to j}$ by evaluating Eq. 61. To this end the integals over E and T are replaced by Gauss-Legendre quadratures:

$$\sigma_{r,n,l}^{g\to j} = \frac{1}{\xi_g}\sum_{a=1}^{Q_E}\sum_{b=1}^{Q_T}\xi(E_a)\sigma_{r,n}(E_a)\mathcal{S}(\mu_c^*)\left|\frac{d\mu_c}{dT}\right| P_i^*(\mu_l^*)w_a w_b \tag{63}$$

The outer loop traverses energies E_a and weights w_a given by:

$$\begin{aligned} E_a &= \frac{E_g - E_{g+1}}{2}x_a + \frac{E_g + E_{g+1}}{2} \\ w_a &= \frac{\omega_a}{2(E_g - E_{g+1})}, \end{aligned} \tag{64}$$

where x_a and ω_a are the a-th abscissa and weight of the Gauss-Legendre quadrature, respectively. The inner loop traverses over T_b, but depending on the value of the group boundaries T_j and T_{j+1}, the computation of the T_b differs:

- Case $\gamma E_a < T_{j+1}$: The lower energy bound of this recoil group is above the maximum possible recoil energy. In this case, no loop needs to be performed and the contribution from this E_a is simply 0.
- Case $T_{j+1} \leq \gamma E_a < T_j$: The maximum possible recoil group is between the lower and upper bound in the recoil group. Set $T_u = \gamma E_a$ and compute:

$$\begin{aligned} T_b &= \frac{T_u - T_{j+1}}{2}x_b + \frac{T_u + T_{j+1}}{2} \\ w_b &= \frac{\omega_b}{2(T_u - T_{j+1})} \end{aligned} \tag{65}$$

This corresponds to rescaling the abscissas and weight to the new range $[T_{j+1}, T_u]$.

- Case $T_j < \gamma E_a$ Set $T_u = T_j$: and use Eq. 65.

9. Analytical Computation of Angular Distribution for Elastic Recoils

In the case of elastic cross recoils, constant neutron energy spectrum, and isotropic scattering in the CM frame, the angular distribution of recoils originating from neutron energy group g and ending up in recoil group t can be computed analytically. It is useful to first consider the case where the neutron and recoil energy groups are very narrow, i.e. contain only a single energy each denoted by E and T, respectively; this corresponds to assume the distibution of neutrons and recoils in energy is a delta function about E or T. In this case, μ_L is given by:

$$\mu_L = \sqrt{\frac{T}{E\gamma}}, \tag{66}$$

and the distribution is also a delta function $p_{\mu_L} = \delta\left(\mu_L - \sqrt{\frac{T}{E\gamma}}\right)$. The scattering cosine depends only on the ratio of T and E so we define:

$$r \equiv \frac{T}{E}. \tag{67}$$

An energy bin for neutrons or recoils represents the population within that energy range by a single number corresponding to the total or average population. The details of the interior distribution are not available so the best representation we have for the distribution of neutrons or recoils in their respective energy bin is uniform. Comparing the situation with the case of a single energy pairing E and T we now consider a case where neutrons within a range ΔE around E can create a recoil in ΔT about T, where the populations are assumed to be uniformly distributed across the respective ranges. The next question is, if E and T are uniformly distributed, what is the distribution of

p_{μ_L}? As μ_L only depends on the ratio of T and E, we can express p_{μ_L} in terms of the distribution of ratios p_r:

$$|p_{\mu_L} d\mu_L| = |p_r dr| \Rightarrow p_{\mu_L} = 2\gamma\mu_L p_r(\gamma\mu_L^2). \tag{68}$$

The distribution p_r is the distribution of the ratio of two uniformly distributed variables T and E. The most convenient way of determining p_r is to first determine the cumulative distribution function (cdf) $P_r(r)$ defined as the probability that a ratio ρ satisfies $\rho < r$. Then the probability density function (pdf) can simply be determined by differentiation $p(r) = \frac{dP_r}{dr}$.

For convenience, we denote the energy ranges by $[E_l, E_u]$ and $[T_l, Tu]$ and define four characteristic ratios:

$$\begin{aligned} r_l &= \frac{T_l}{E_l} \\ r_u &= \frac{T_u}{E_u} \\ r_{min} &= \frac{T_l}{E_u} \\ r_{max} &= \frac{T_u}{E_l} \end{aligned} \tag{69}$$

The cdf can be most easily determined by geometrical considerations. If E and T are plotted as x and y axes, respectively, $T = rE$ is a line containing the origin, and $\rho < r$ is the area underneath the line. The probability of of a recoil event from $[E_l, E_u]$ to $[T_l, T_u]$ is the intersection of the area under the line $T = rE$, and the quadrilaterial defined by $[E_l, E_u] \times [T_l, T_u]$ divided by the area of the box $(E_u - E_l)(T_u - T_l)$. Hence, the computation of $P_r(r)$ reduces to computing the area that hte line $T = rE$ cuts out of the quadrilateral $[E_l, E_u] \times [T_l, T_u]$. The cdfs are given by:

Case 1: $r_u < r_l$

$$P_r(r) = \begin{cases} 0 & r < r_{min} \text{ or } r \geq r_{max} \\ \frac{rE_u^2 - 2T_l E_u + \frac{T_l^2}{r}}{2\Delta E \Delta T} & r_{min} \leq r < r_u \\ \frac{E_u - \frac{1}{2r}(T_l + T_u)}{\Delta E} & r_u \leq r < r_l \\ 1 - \frac{\frac{T_u^2}{r} - 2T_u E_l + E_l^2 r}{2\Delta E \Delta T} & r_l \leq r < r_{max} \end{cases}$$

Case 2: $r_u = r_l$

$$P_r(r) = \begin{cases} 0 & r < r_{min} \text{ or } r \geq r_{max} \\ \frac{rE_u^2 - 2T_l E_u + \frac{T_l^2}{r}}{2\Delta E \Delta T} & r_{min} \leq r < r_l \\ 1 - \frac{\frac{T_u^2}{r} - 2T_u E_l + E_l^2 r}{2\Delta E \Delta T} & r_l \leq r < r_{max} \end{cases}$$

Case 3: $r_u > r_l$

$$P_r(r) = \begin{cases} 0 & r < r_{min} \text{ or } r \geq r_{max} \\ \frac{rE_u^2 - 2T_l E_u + \frac{T_l^2}{r}}{2\Delta E \Delta T} & r_{min} \leq r < r_l \\ \frac{\frac{1}{2}r(E_u + E_l) - T_l}{\Delta T} & r_l \leq r < r_u \\ 1 - \frac{\frac{T_u^2}{r} - 2T_u E_l + E_l^2 r}{2\Delta E \Delta T} & r_u \leq r < r_{max} \end{cases}$$

The pdfs are given by:

Case 1: $r_u < r_l$

$$p_r(r) = \begin{cases} 0 & r < r_{min} \text{ or } r \geq r_{max} \\ \frac{E_u^2 - \frac{T_l^2}{r^2}}{2\Delta E \Delta T} & r_{min} \leq r < r_u \\ \frac{T_l + T_u}{2\Delta E r^2} & r_u \leq r < r_l \\ \frac{\frac{T_u^2}{r^2} - E_l^2}{2\Delta E \Delta T} & r_l \leq r < r_{max} \end{cases}$$

Case 2: $r_u = r_l$

$$p_r(r) = \begin{cases} 0 & r < r_{min} \text{ or } r \geq r_{max} \\ \frac{E_u^2 - \frac{T_l^2}{r^2}}{2\Delta E \Delta T} & r_{min} \leq r < r_l \\ \frac{\frac{T_u^2}{r^2} - E_l^2}{2\Delta E \Delta T} & r_l \leq r < r_{max} \end{cases}$$

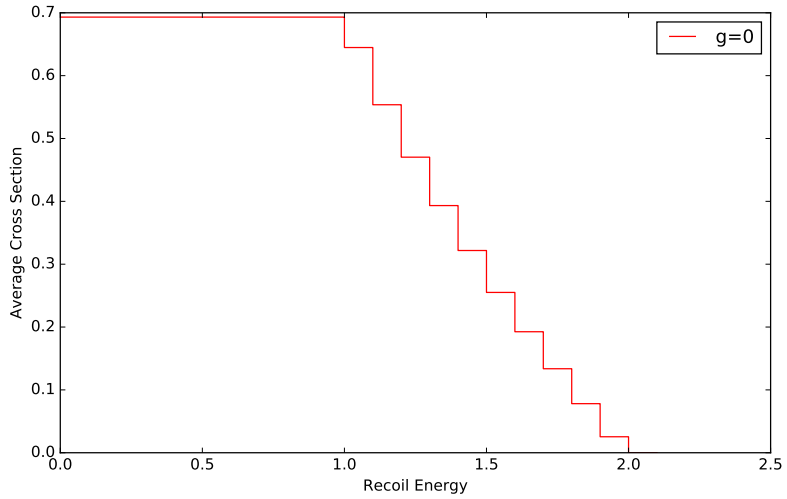

Figure 5: Average recoil cross section of ^{1}H given constant scattering cross section and spectrum, $1 < E < 2$.

Case 3: $r_u > r_l$

$$p_r(r) = \begin{cases} 0 & r < r_{min} \text{ or } r \geq r_{max} \\ \frac{E_u^2 - \frac{T_l^2}{r^2}}{2\Delta E \Delta T} & r_{min} \leq r < r_l \\ \frac{E_u + E_l}{2\Delta T} & r_l \leq r < r_u \\ \frac{\frac{T_u^2}{r^2} - E_l^2}{2\Delta E \Delta T} & r_u \leq r < r_{max} \end{cases}$$

Using $p_r(r)$ in Eq. 68 yields the distribution of recoils over μ_L. Note that we approximated the distribution of neutrons and recoils within their respective bins as uniform, which is not exactly what the multigroup formalism corresponds to. In fact, multigroup formalism simply means that all we keep track of is the average (or equivalently the total) and we do not retain information of the within-bin distribution of neutrons or recoils. However, the obtained results are still useful for small bins as the population becomes better approximated by a constant function ($O(\Delta E)$, $O(\Delta T)$).

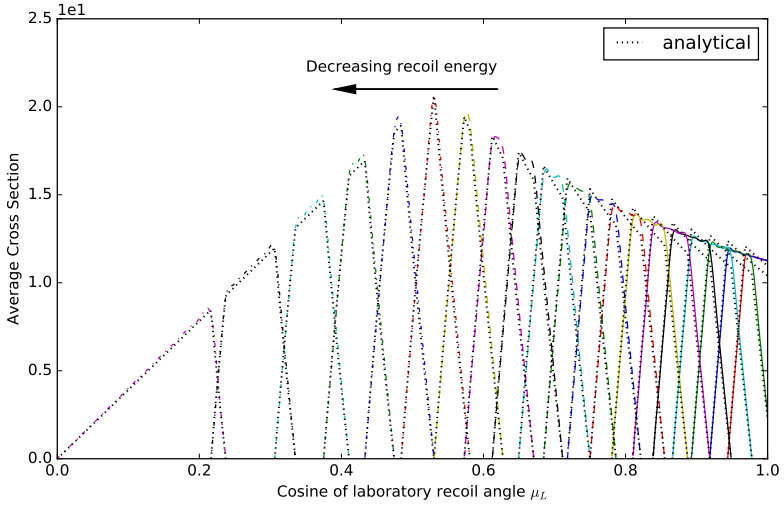

Figure 6: Value of the transfer cross section from neutron energy group $g = 0$ to various recoil energy groups indexed by t.

10. Verification of Elastic Scattering Cross Sections

The first test uses a constant spectrum $\xi(E) = 1$, constant recoil cross section $\sigma_{r,n}(E) = 1$, hydrogen with $A = 1$ as recoil nucleus. We focus on a neutron energy bounded by $E = [0, 1]$ eV. The recoil energy groups have a width of 0.1 eV and are uniformly distributed from 0 to 2 eV; L is set to 0. The expectation is that the average recoil cross section increases linearly between $1 < T < 2$ and remains constant between $0 < T < 1$. Figure 5 shows the result obtained with the cross section preparation object behaves as expected.

The second test is to assert correctness of the computed angular distribution in the LAB frame. To this end, we compare results from the implemented algorithm with analytical results derived in section 9. To reduce impact of wide energy bins, we use $1 < E < 1.2$ and $\frac{j-1}{20} < T < \frac{j}{20}$ for $j = 1, ..., 20$. We select $A = 2$ corresponding to $\gamma = 8/9$.

In Fig. 6, the value of the transfer cross section is plotted vs. the LAB scattering cosine μ_l. The black dotted lines are the analytical reference for

$j = 1, .., 20$ while the colorized lines are the results from the computation for $L = 20$. The index j of the curves increases from left to right as larger j correspond to smaller energy transfer; in turn smaller energy transfer to the recoil corresponds to smaller LAB scattering cosines as shown in Eq. 55. This behavior is reproduced in Fig. 6. The analytical results are in good agreement with the computed distributions. It should be noted that the angular distributions p_{μ_L} are not continously differentiable leading to relatively slow convergence of the numerical results to the analytical solution with increasing L.

11. Preliminary Cross Sections for Inelastic Scattering

The first test uses ^{1}H, $\xi(E) = 1$, $\sigma_{r,n}(E) = 1$, and three values for Q : 0.1, 0.4, 0.8. Neutron energy groups are set to $E_0 = [1, 2]$, $E_1 = [0, 1]$ and recoil energy groups are given by $T_j = [2 - \frac{j}{20}, 2 - \frac{j-1}{20}]$, $j = 1, .., 20$. The average neutron to recoil energy group transfer cross section is depicted in Figs. 7 to 9 for $Q = 0.1$, $Q = 0.4$, and $Q = 0.8$, respectively. The neutron and recoil energy limits that apply to this problem are collected in Fig. 2. We observe that the results in Figs. 7 to 9 abide by the limits in the table. Why maximum in the middle?

The second test investigates the angular distribution for $Q = 0.2$, $A = 2$, $E = [1.0, 1.2]$, and $T_j = [1 - \frac{j}{20}, 1 - \frac{j-1}{20}]$, $j = 1, ..., 10$. The results are plotted in Fig. 10. First, the lower limit of LAB cosines in Fig. 10 is observed to be $\mu_{L,\downarrow} = 0.5$. From Eq. 40 we find that in this case with $E_t = 0.3$ and $E_\uparrow = 1.2$, we have $\mu_{L,\downarrow} = \sqrt{0.3/1.2} = 0.5$.

The peculiar shape of the lowest recoil energy group needs to discussed. The $E = 1$ line in a plot totally equivalent to Fig. 4 would be the locus of $\mu_{L,\uparrow}$. The curves are relatively flat for $T > \frac{|Q_j|}{A+1}$ but steep for $T < \frac{|Q_j|}{A+1}$. In our case, we have $frac|Q_j|A + 1 \approx 0.067$ such that only the lowest energy group is significantly to the left of the maximum. The minimum recoil energy of the lowest energy group results in the largest $\mu_{L,\uparrow}$ which in this case is $\mu_{L,\uparrow} = 1$. The seemingly unexpected change in shape from the $T = [0.05, 0.1]$ to the

$T = [0, 0.05]$ recoil energy group is caused by the steepness of the μ_L vs. T curve with the additional complication of only the lowest recoil energy group having energies in this range. To resolve the steepness of the LAB recoil cosine curve, more recoil energy groups would be required, i.e. then we would see a smooth return of $\mu_{L,\uparrow}$ from low values to higher values and finally to 1. As low recoil energy groups are inconsequential, it is recommended to cut off the recoil energies below $\frac{|Q_j|}{A+1}$. Note that the higher A is the lower Q_j tends to be and in this case $\frac{|Q_j|}{A+1}$ will be even smaller.

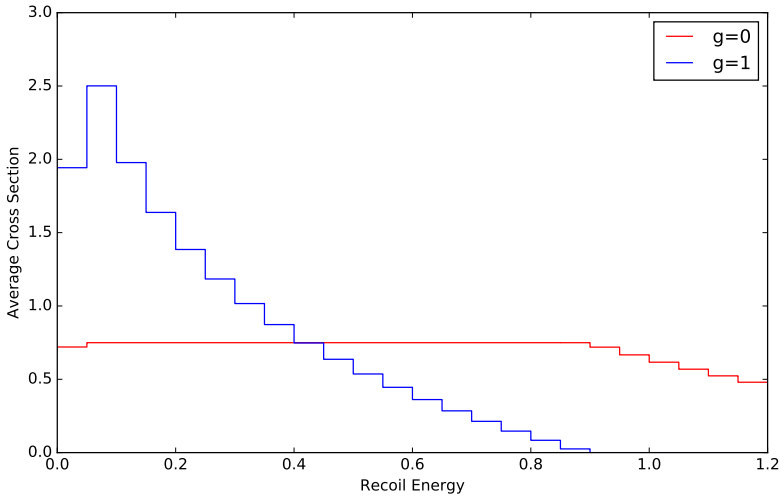

Figure 7: Average recoil cross section of ^{1}H given constant scattering cross section and spectrum, $g = 0: \ 1 < E < 2, \ g = 1: \ 0 < E < 1, \ Q = 0.1$.

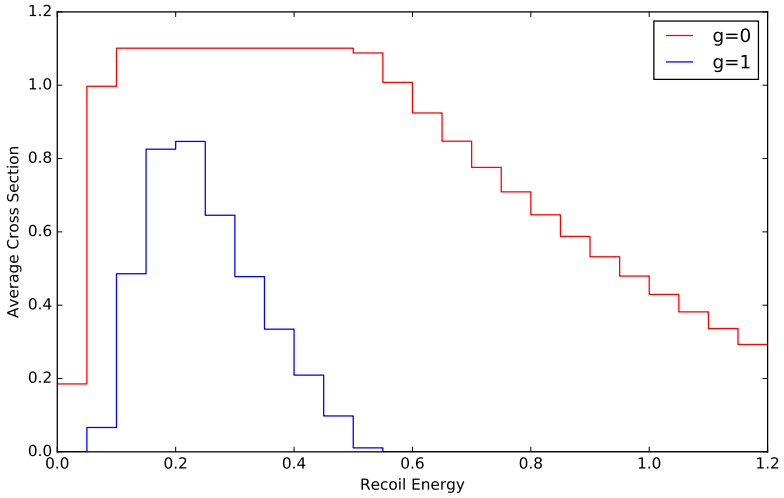

Figure 8: Average recoil cross section of ^{1}H given constant scattering cross section and spectrum, $g = 0: \ 1 < E < 2, \ g = 1: \ 0 < E < 1, \ Q = 0.4$.

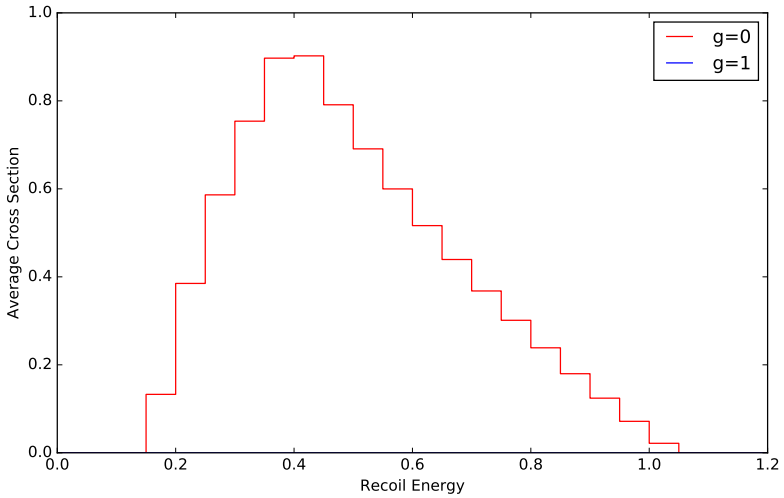

Figure 9: Average recoil cross section of ^{1}H given constant scattering cross section and spectrum, $g = 0: \ 1 < E < 2, \ g = 1: \ 0 < E < 1, \ Q = 0.8$.

Table 2: Minimum and maximum neutron and recoil energies for inelastic scattering test problem.

	Q	0.1	0.4	0.8
	E_t [Eq. 15]	0.2	0.4	1.6
$g = 0$	E_{min}	1	1	1.6
	E_{max}	2	2	2
	T_{min} [Eq. 33]	0.0013	0.025	0.153
	T_{max} [Eq. 33]	1.899	1.575	1.047
$g = 0$	E_{min}	0.2	0.8	-
	E_{max}	1	1	-
	T_{min} [Eq. 33]	0.0028	0.077	-
	T_{max} [Eq. 33]	0.897	0.524	-

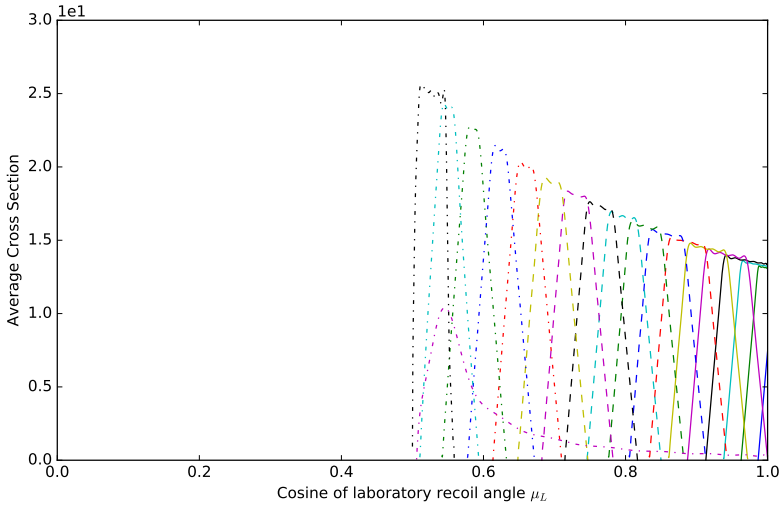

Figure 10: Angular distribution of recoils for inelastic scattering events from $E = [1, 1.2]$ to $T_j = [1 - \frac{j}{20}, 1 - \frac{j-1}{20}]$, $j = 1, ..., 10$, with $A = 2$, $Q = 0.2$.

References

[1] National nuclear data center, http://www.nndc.bnl.gov/index.jsp, accessed: 2018-01-23.

[2] Y. Wang, S. Schunert, V. Laboure, Rattlesnake Theory Manual, INL (2017).

[3] Fundamentals of radiation materials science: Metals and alloys, Springer Berlin Heidelberg, 2007. doi:10.1007/978-3-540-49472-0.

[4] J. J. Duderstadt, L. J. Hamilton, Nuclear Reactor Analysis, John Wiley & Sons, Inc.

[5] E. E. Lewis, W. F. Miller, Computational Methods of Neutron Transport, John Wiley & Sons.